Received: 22 January 2018 | Revised: 17 April 2018 | Accepted: 9 May 2018

DOI: 10.1002/joc.5714

International Journal of Climatology RMetS

RESEARCH ARTICLE

High-resolution projection of climate change and extremity over Israel using COSMO-CLM

Assaf Hochman[1,2,3] | Paola Mercogliano[4,5] | Pinhas Alpert[1] | Hadas Saaroni[3] | Edoardo Bucchignani[4,5]

[1]Department of Geosciences, School of Geosciences, Tel Aviv University, Tel-Aviv, Israel

[2]Porter School of Environmental Studies, School of Geosciences, Tel-Aviv University, Tel-Aviv, Israel

[3]Department of Geography and the Human Environment, School of Geosciences, Tel-Aviv University, Tel-Aviv, Israel

[4]CMCC Euro-Mediterranean Center on Climate Change, Capua, Italy

[5]CIRA Centro Italiano Ricerche Aerospaziali, Capua, Italy

Correspondence
Assaf Hochman, Department of Geosciences, School of Geosciences, Tel-Aviv University, Tel-Aviv 69978, Israel.
Email: assafhochman@post.tau.ac.il; assafhochman@yahoo.com

Funding information
German Helmholtz Association; Ministry of Science and Technology (MOST); Italian Ministry of the Environment, Land and Sea; Italian Ministry of Education

High-resolution climate projections over Israel (about 8 km) have been obtained with the regional model COSMO-CLM, nested into the CORDEX-MENA simulations at 25 km resolution. This simulation provides high-resolution spatial variability of total precipitation and precipitation intensity. Projections are presented not only in terms of average properties, but also using a subset of extreme temperature and precipitation indices from the standard Expert Team on Climate Change Detection and Indices (ETCCDI) for the period 2041–2070 with respect to 1981–2010 (RCP4.5).

A general increase in seasonal mean temperature is projected throughout the domain with peaks of ~2.5 °C, especially in winter and autumn. Extreme temperature indices show increases, larger in the minimum than in the maximum temperatures. Regarding total seasonal precipitation, decreases were found in the north and central Mediterranean climate parts of Israel, with reductions reaching ~40%, and increases of the same percentage in the most southern arid parts during winter and spring. An increase in precipitation intensity is shown mostly for the southern arid part of the region, with some indications of extremity also in the north. This spatial pattern probably results from a decrease in cyclones' occurrences, which mainly influences the northern and central parts of Israel, and an increase in convective activity in the south.

The outcome of this study can serve as a basis for priority setting and policy formulation towards better climate adaptation.

KEYWORDS

COSMO-CLM, downscaling, eastern Mediterranean, ETCCDI, extreme precipitation, extreme temperature, Israel, RCM

1 | INTRODUCTION

Future prediction of local hazards can be performed mainly through outputs of climate models. While global circulation models (GCMs) are a most comprehensive tool for studying climate conditions and even local regimes, they have often been criticized when used for modelling the complex climate regime of the Mediterranean region (e.g., Lionello *et al.*, 2014). The main concern is the coarse resolution of the models that is problematic in identifying mesoscale processes and especially local weather conditions due to the complex terrain of the Mediterranean region. This issue is important, and problematic, when aiming to represent precipitation and temperature extremes in the eastern Mediterranean (EM), the Levant region and Israel. In order to bridge the gap between GCM's and simulations of local climatic variables, downscaling methods were developed (Wilby and Wigley, 1997), as for example, the statistical downscaling

for precipitation in Israel, performed by Alpert *et al.* (2008) and Rostkier-Edelstein *et al.* (2015).

There are two main approaches for downscaling GCMs; the first is a statistical approach known to be less computationally demanding; developing statistical relations between grid points of GCMs and observed local atmospheric conditions. The second is a dynamical approach; GCM outputs are used to force regional climate models (RCMs) that can better represent the physical and dynamical characteristics of the specific region due to their higher resolution (Giorgi and Gutowski, 2015).

The strategy of dynamical downscaling, adopted in this study, appears to be especially challenging and important for simulating local climate features in the EM and Israel and for supporting impact studies over the whole area (also where observations are not available for the development of statistical downscaling). The EM climate conditions are characterized by moderate air temperatures during the rainy winter season and dry and stable hot weather conditions during summer. The region's climate is intensely affected by external forcing of both mid-latitude and tropical origins (e.g., Alpert *et al.*, 2005). The rain regime is characterized by relatively limited number of rainy days, that is, relatively high intensity of rain, with large inter- and intra-seasonal variations. While rainy events are typically associated with intrusions of cold air masses of north European origin that pass over the warm water of the Mediterranean Sea (Alpert and Reisin, 1986), the other days are characterized by prolonged dry conditions (Saaroni *et al.*, 2015) including polar cold and dry intrusions (Saaroni *et al.*, 1996). Penetration of warm humid masses originating from tropical Atlantic and/or equatorial regions of eastern Africa and the Arabian Sea also appear during the winter and the transitional seasons (Krichak *et al.*, 2004; 2015; Ziv *et al.*, 2005; De Vries *et al.*, 2013). Topographical (local) and coastal (mesoscale) effects (e.g., land–sea breezes) influence the spatial distribution of climate features in this region (Krichak *et al.*, 2010). Such effects are especially notable in the mountainous and immediate coastal areas of the EM (Hochman *et al.*, 2017a).

Extreme weather events have vast environmental implications in the Levant with essential influence on human life, economy and ecosystems (Ziv *et al.*, 2014; Kelley *et al.*, 2015). While monthly means provide useful climatological information to detect slow climate change processes, environmental impacts are often the result of short-term phenomena occurring well into the distribution tails of daily data (Zhang *et al.*, 2011). To gain a uniform perspective on changes in weather and climate extremes, an internationally coordinated core set of 27 indices of temperature and precipitation extremes was defined by the Expert Team on Climate Change Detection and Indices (ETCCDI; Klein-Tank *et al.*, 2009; Zhang *et al.*, 2011). These extreme indices have multiple applications in climate research due to their robustness and have been widely used for analyzing past and future trends in extremes (e.g., Samuels *et al.*, 2011; Smiatek *et al.*, 2011; Soares *et al.*, 2012; Dominguez *et al.*, 2013; Turco *et al.*, 2013; Zollo *et al.*, 2016; Samuels *et al.*, 2017; Zittis, 2017).

Samuels *et al.* (2017) have evaluated the ability of 23 models, participating in the Coupled Model Intercomparison Project phase 5 (CMIP5), to predict extreme precipitation indices (EPI) in the 21st century over the EM. Overestimations in EPIs were observed in CMIP5 models as compared to observations. These overestimations were related to the inadequate representation of topography in the GCMs, due to relatively coarse spatial resolutions. Furthermore, the above mentioned authors concluded that while total precipitation is projected to decrease, extreme precipitation is projected to increase, at least for the Fertile Crescent region. Such a trend has been shown over the Mediterranean region for the second half of the 20th century (Alpert *et al.*, 2002; Zhang *et al.*, 2005; Yosef *et al.*, 2009; Ziv *et al.*, 2014), though insignificant for the Middle East and Israel, attributed to the high inter-annual variability of precipitation in this region.

Following Hochman *et al.* (2017a) the main purpose of this study is to employ the COSMO-CLM model in dynamically downscaling the CMCC-CM global model to an 8 km grid resolution over the region of Israel, in order to project average and extreme changes in precipitation and temperature until 2070. In that work, in fact, authors have showed that increasing the spatial resolution of the COSMO-CLM model, from 50 to 8 km, improves the simulation of extreme precipitation and temperatures over Israel, due to better representation of the complex terrain and of the location of land and sea in the model. Furthermore, Hochman *et al.* (2017a) stressed that improvement in the simulation of precipitation and temperature due to increased spatial resolution of the model is mostly found for the very local scale station observations and especially in the simulation of daily extremes and less for seasonal and spatial averages in gridded data sets.

2 | DATA AND SETUP OF EXPERIMENT

The RCM used in this study is COSMO-CLM (Rockel *et al.*, 2008), which is the climate version of the three-dimensional, non-hydrostatic mesoscale weather forecast model COSMO-LM (Steppeler *et al.*, 2003; Baldauf *et al.*, 2011).

The RCM COSMO-CLM has been used to perform two simulations over the Coordinated Regional Downscaling Experiment Middle East North Africa (CORDEX-MENA; e.g., Ozturk *et al.*, 2018; Bucchignani *et al.*, 2018) domain (Figure 1a; 27°W–76°E, 7°S–45°N) defined in the frame of the CORDEX initiative (Giorgi *et al.*, 2009) at spatial resolutions of 0.44° (~50 km) and 0.22° (~25 km). The domain includes North Africa, southern Europe and the whole

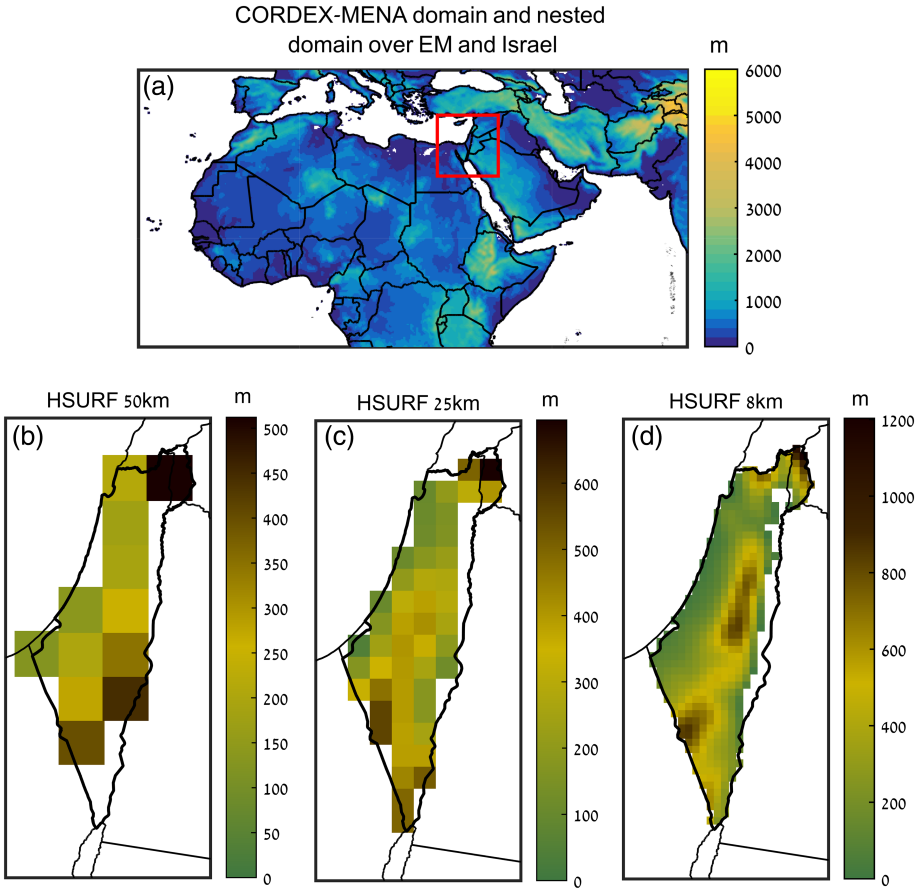

FIGURE 1 CORDEX-MENA domain and the nested domain of 8 km resolution (a) and topography in the three nested grids of the COSMO-CLM model at 50 (b), 25 (c) and 8 km (d) resolutions. HSURF is the elevation above sea level in the model. Results in this study were evaluated only over Israel [Colour figure can be viewed at wileyonlinelibrary.com]

Arabian Peninsula, offering considerable challenges for assessing and understanding future local climate change, due to its large size, including highland areas, wide coastal areas and deserts.

An optimized model configuration, after a sensitivity analysis, was adopted (Bucchignani *et al*., 2016a), which uses the parameterization of albedo derived from the Moderate Resolution Imaging Spectroradiometer (MODIS) data (Lawrence and Chase, 2007), which more realistically describes the Earths' surface reflectivity. Also, the National Aeronautics and Space Administration Goddard Institute for Space Studies Aerosol Optical Depth (NASA-GISS AOD) distribution (Tegen *et al*., 1997) and the Tiedtke Cumulus Convection parameterization were used (Tiedtke, 1989). The domain includes a relaxation zone of at least 15 grid points from each side and the first year of simulation (1979) was removed, as the spin-up period is influenced by initial conditions, following the methodology already employed in previous studies (e.g., Zollo *et al*., 2016). Accordingly, climate projections over the 21st century have been conducted (Bucchignani *et al*., 2018) adopting the same spatial resolutions. The future projections are performed under the IPCC representative concentration pathway 4.5 (RCP4.5) scenario (Moss *et al*., 2010), which assumes that greenhouse gases will increase and peak around 2040, and then will start to decline. Initial and boundary conditions were derived by the global climate model CMCC-CM (Scoccimarro *et al*., 2011), which was found to represent EPI in the EM relatively well (Samuels *et al*., 2017).

Successively, a high-resolution simulation over a domain encompassing Israel has been performed at a 0.0715° resolution (~8 km, named ISR8, hereafter), nested into the 0.22° resolution simulation (~25 km) in order to project climate changes until 2070. The 8 km simulation is performed over the domain shown in Figure 1a (the embedded rectangle), which is larger than the region of Israel. It is standard practice to perform simulations over domains larger than the area of interest, in order to reduce boundary effects. Then, results were analysed only over Israel (Figure 1b–d). Validation results under perfect boundary conditions, that is, derived from ERA-Interim reanalysis have been presented in Hochman *et al*. (2017a). The models' topography at the different spatial resolutions, 50, 25 and 8 km, is shown in Figure 1b–d, respectively.

In the present work, the model output for ISR8 driven by CMCC-CM is validated against E-OBS and APHRODITE data sets in terms of seasonal bias in the average climate

properties. E-OBS (Haylock *et al*., 2008) is a widely used gridded data set of precipitation and temperature at a 0.25° spatial resolution, available for the period 1980–2011. It has been designed to provide the best estimate of grid box averages, to enable direct comparison with RCMs (Tanarhte *et al*., 2012). Here, E-OBS was used to evaluate mean temperature biases. It should be noted that recent studies have shown that the E-OBS data set tends to underestimate precipitation in the EM region, especially during very wet days (Zittis *et al*., 2017). The APHRODITE data (Yatagai *et al*., 2008; 2012), is a gridded data set at a 0.25° spatial resolution, of daily precipitation over the EM region, for the period 1980–2004, whereas over Israel the database has a much higher spatial resolution (~5 km). This data set is based on a dense network of rain gauges in the Middle East, already proven to serve as a good evaluating tool for climate models performance. In addition, when APHRODITE was compared to other gridded data sets it demonstrated the effects of orography on precipitation (Yatagai *et al*., 2008).

Finally, climate projections in terms of seasonal averages of precipitation, temperature and extreme climate indicators, for 2041–2070 and the reference period 1981–2010, were investigated over Israel. The extreme indices considered in the present study represent a subset of the standard ETCCDI ones. Six temperature and eight precipitation indices (Tables 1 and 2, respectively) have been selected, previously evaluated in Hochman *et al*. (2017a).

3 | RESULTS

3.1 | Evaluation of seasonal mean temperature and precipitation

Spatial patterns of seasonal mean temperature bias for ISR8 with respect to E-OBS for 1980–2011 are presented in Figure 2. General underestimations, that is, colder model, are found especially in the winter (DJF) seasonal temperatures, inherited from the driving GCM (CMCC-CM; Bucchignani *et al*., 2018), whereas some overestimations (model is warmer) are found in the eastern parts of Israel in the summer (JJA). Because the maximum daily temperature during the summer is governed by the Etesian winds together with the sea–land breeze circulation (Levi *et al*., 2011), it is speculated here that the 8 km simulation does not adequately represent the cool sea–land breeze winds, thus producing overestimations, which are probably smoothed out in the mean daily temperatures (Hochman *et al*., 2017a). However, because the Etesian winds are a larger-scale phenomenon, they are probably simulated well by the RCM simulation (e.g., Dafka *et al*., 2017). Other feedbacks within the model may be responsible for the overestimation of seasonal temperatures, such as the soil moisture–air temperature coupling (e.g., Seneviratne *et al*., 2010; Zittis *et al*., 2014).

TABLE 1 List of indicators considered for temperature

Label	Description	Units
SU	Summer days—annual count of days when the daily T_{max} is above 25°	days/year
90p T_{max}	90th percentile of daily T_{max}	°C
TXx	Annual maximum value of daily T_{max}	°C
TR	Tropical nights—annual count of days when the daily T_{min} is above 20°	days/year
10p T_{min}	10th percentile of daily T_{min}	°C
TNn	Annual minimum value of daily T_{min}	°C

The negative temperature biases (Figure 2) matching the positive precipitation ones (Figure 3) hints at this.

Spatial patterns of seasonal precipitation bias for ISR8 against APHRODITE for 1980–2004 are presented in Figure 3. Generally, a west–east pattern of overestimations in the coastal plains and underestimations in the mountainous regions is found in the seasonal precipitation, especially in the winter months (DJF). Furthermore, for the summer season (JJA), in which no significant precipitation events occur, simulations do not show any bias, indicating their good skill. Seasonal temperature and precipitation biases of the CMCC-CM model and the 0.44 and 0.22° simulations over the entire MENA-CORDEX domain were earlier presented in Bucchignani *et al*. (2018).

The above mentioned findings for both the seasonal mean bias in temperature and precipitation are consistent with the results of Hochman *et al*. (2017a), which extensively evaluated the ISR8 simulation, under perfect boundary conditions, driven by ERA-Interim reanalysis.

3.2 | Projections of seasonal mean temperature and precipitation

Surface air (2 m) temperature and precipitation are the most basic climatic variables with large environmental implications. Even if extremes can have larger environmental impacts, projection of the seasonal means is important and is a pre-condition for in depth further analysis of extremes.

TABLE 2 List of indicators considered for precipitation

Label	Description	Units
SDII	Mean precipitation on wet days (>1 mm)	mm/day
CWD	Maximum number of consecutive wet days (>1 mm)	days/year
Rx1day	Maximum of daily precipitation	mm/day
R10	Number of days with precipitation ≥10 mm/day	days/year
R20	Number of days with precipitation ≥20 mm/day	days/year
99p	99th percentile of daily precipitation	mm/day
90p	90th percentile of daily precipitation	mm/day
CDD	Maximum number of consecutive dry days (<1 mm)	days/year

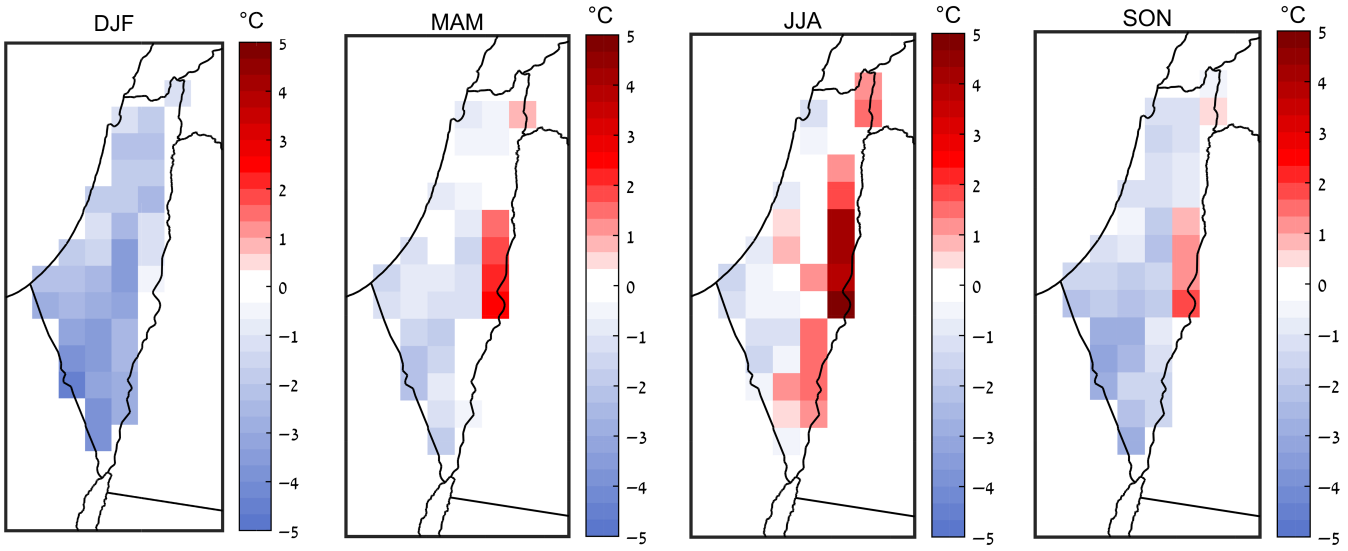

FIGURE 2 ISR8 seasonal mean temperature bias (°C) with respect to E-OBS for 1980–2011 [Colour figure can be viewed at wileyonlinelibrary.com]

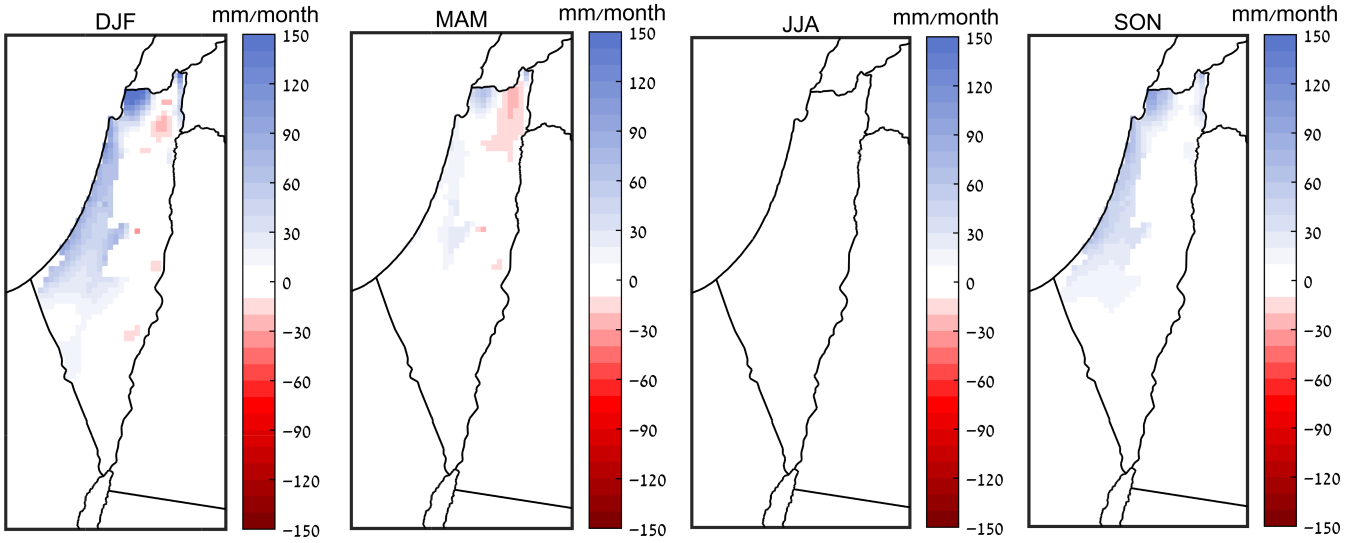

FIGURE 3 ISR8 seasonal precipitation bias in mm/month, with respect to APHRODITE for 1980–2004 [Colour figure can be viewed at wileyonlinelibrary.com]

Figure 4 presents ISR8 projections of seasonal temperature and precipitation as a difference between 2041–2070 and 1981–2010, under RCP4.5 scenario. A pronounced increase in the mean temperature is predicted throughout the entire domain with peaks of up to ~2.5 °C (Figure 4, top row). The largest increase appears in the autumn (SON) and in the winter (DJF). In spring (MAM) a west–east gradient is found showing larger temperature increases in the eastern part of the domain as compared with the western part, a trend seen also for the autumn, and partly for the winter. However, in the summer (JJA), a north–south gradient takes place with a larger temperature increase in the southern half of Israel, that is, the semi-arid and arid regions. It is worth noting that in the recent decades the strongest warming was observed in summer and weakest in the winter (Ziv *et al.*, 2014). Till the 1990s even some cooling in the winter was observed in contrast to significant summer warming (Ben-Gai *et al.*, 1999). Furthermore, earlier GCM and RCM projections of mean seasonal temperatures in the MENA domain (e.g., Laprise *et al.*, 2013; Lelieveld *et al.*, 2016; Ozturk *et al.*, 2018) have suggested that the strongest increase in mean temperature will take place in the summer season using ≥50 km resolution simulations. Hochman *et al.* (2017a) have showed that the higher 8 km resolution better reproduces the maximum temperature, due to better simulation of the sea–land breeze, especially in summer. This might explain the slightly smaller increase in temperature during the summer, when the sea–land breeze is most effective as opposed to the winter and autumn seasons. The breeze might be strengthening in a warmer climate due to the different rates of land and sea warming (Alpert *et al.*, 2006; Sutton *et al.*, 2007).

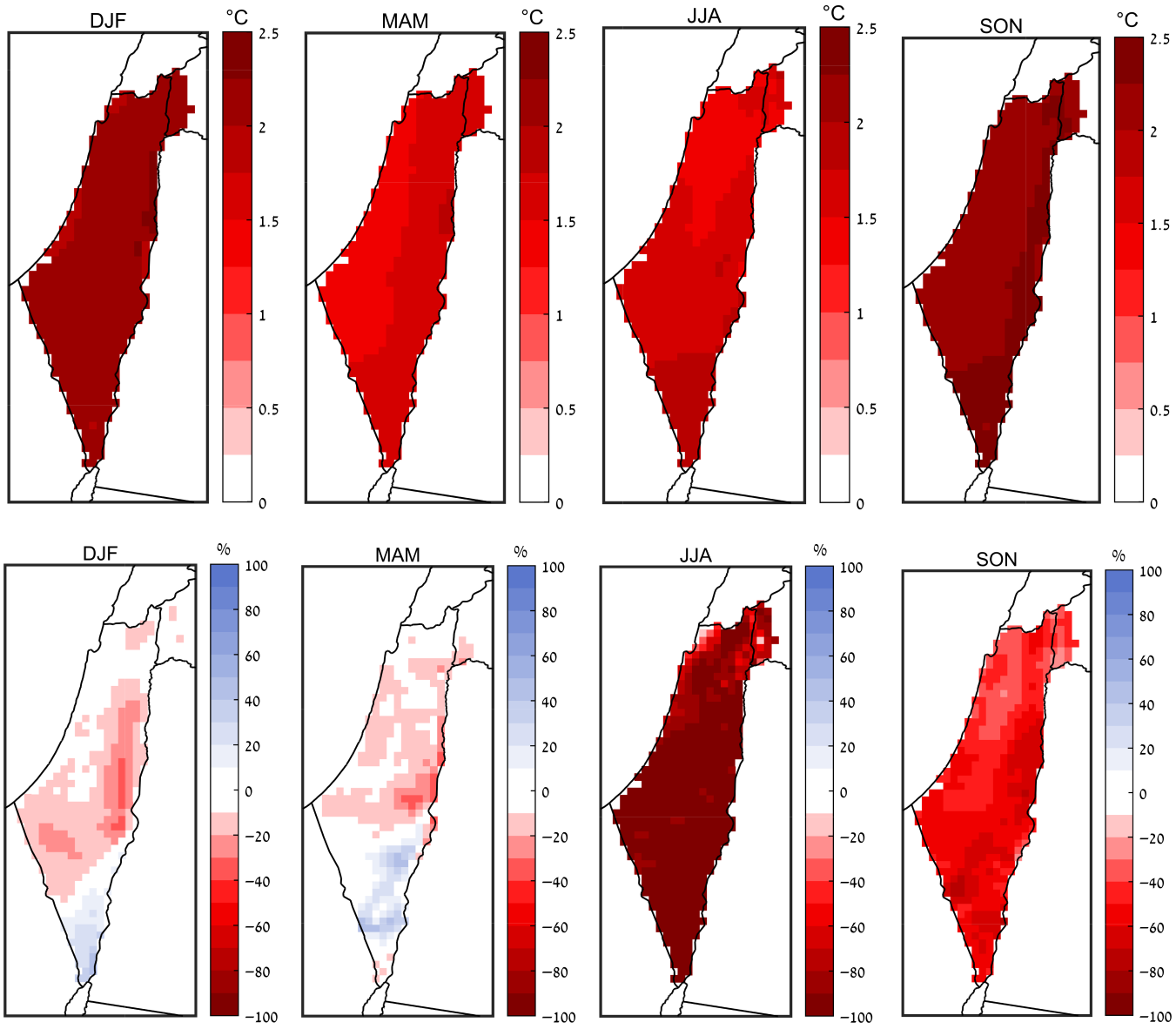

FIGURE 4 ISR8 projected change in seasonal mean temperatures (top row, in °C) and precipitation (bottom row, in %), for 2041–2070 minus 1981–2010, under RCP4.5 scenario [Colour figure can be viewed at wileyonlinelibrary.com]

Regarding precipitation (Figure 4, bottom row), a general decrease is well noted over most parts of the domain, covering the entire study area for the autumn (SON); a reduction reaching ~40%. However, increases are noted in the most southern arid part for winter (DJF) and spring (MAM). The dominant reduction trend may be explained by two global to large-scale mechanisms. The first one is the expected expansion of the Hadley Cell towards the Poles in a warmer climate, a trend that is already being observed (Held and Soden, 2006; Lu *et al*., 2007; Seidel *et al*., 2008). The second one is the increase in the occurrence of the positive phase of the NAO that is associated with northwards migration of the east Atlantic/European cyclone tracks during winter (Eichler *et al*., 2013; Tamarin-Brodsky and Kaspi, 2017). The projected migration of synoptic systems northwards finds expression in the increase of Red Sea Trough (RST) frequencies (Hochman *et al*., 2017c).

Note that ISR8 produces close to zero precipitation during the summer (JJA); therefore, there is a large difference between the two periods because very small changes present very large differences percentage-wise (Figure 4).

3.3 | Projections of extreme temperatures and precipitation

Figure 5 presents the projections for various extreme temperature indicators (ETI), through the differences of 2041–2070 and the reference period 1981–2010, as simulated by ISR8. A pronounced increase is found in all ETIs. Note that the increase in the annual minimum temperature (TNn) is larger than that of the annual maximum temperature (TXx).

Regarding EPI an interesting and complex spatial pattern arises from the high-resolution simulation shown here for the first time (Figure 6). The mean precipitation of wet days

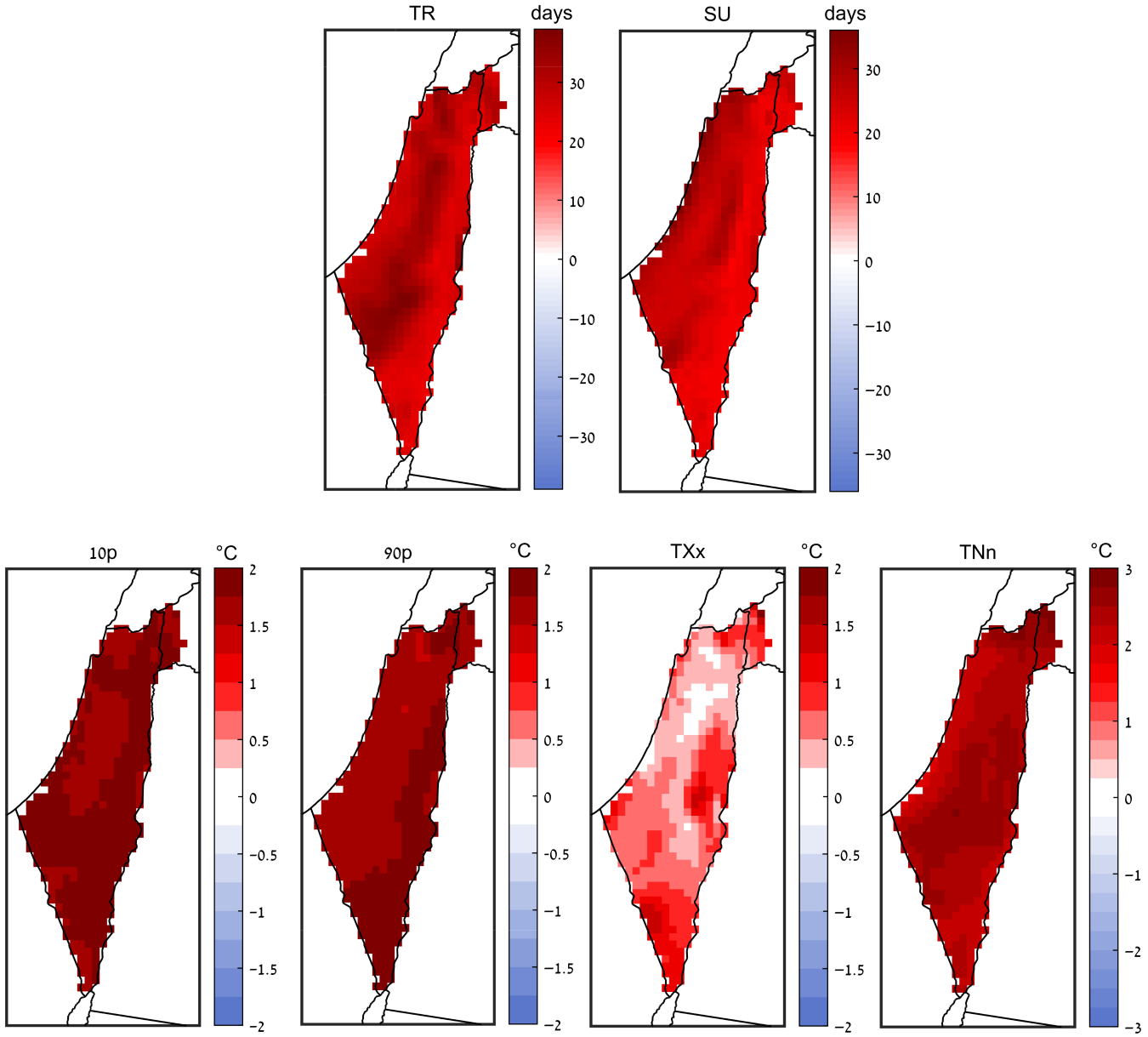

FIGURE 5 ISR8 projections for extreme temperature indicators, 2041–2070 minus 1981–2010, under RCP4.5 scenario. Tropical nights (TR), summer days (SU), 10th percentile of daily T_{min} (10p), 90th percentile of daily T_{max} (90p), annual maximum value of daily T_{max} (TXx), annual minimum value of daily T_{min} (TNn) [Colour figure can be viewed at wileyonlinelibrary.com]

(>1 mm; SDII) is projected to decrease in the northern and central parts of the country while an increase is shown for the most southern arid part, in agreement with the results for the seasonal rainfall of winter and spring (see Figure 4, bottom row). A most similar pattern is seen for the 90th percentile of daily precipitation (90p) that is projected to decrease in the north and central parts of Israel and increase in the southern part by ~8 mm/day. However, the 99th percentile of daily precipitation (99p) is projected to decrease in the centre of the country, but to increase in the northern and southern parts, by ~20 mm/day. The maximum of daily precipitation (Rx1day) shows a similar spatial pattern as the 99p, that is, an increase of ~15 mm/day in the northern and southern parts of the country. This goes along with the paradoxical increase in extreme daily precipitation in spite of decrease in total rainfall over the Mediterranean as reported by Alpert *et al.* (2002).

The consecutive wet days (CWD) index is projected to decrease by about 2 days in the north of Israel and about 1 day in the central and southern parts of the country. The number of days exceeding the 10 and 20 mm thresholds (R10 and R20, respectively) are projected to decrease by 3–4 days. The consecutive dry days (CDD) index is projected to increase by ~20 days in most of the study region, except for a slight increase especially in the central mountainous region and in the northern coastal part of the country. This is in accordance with the projection of a shorter winter and longer summer due to the projected significant decrease in the occurrence of Cyprus Lows and the projected increase in the frequency of the Persian Trough, shown by Hochman

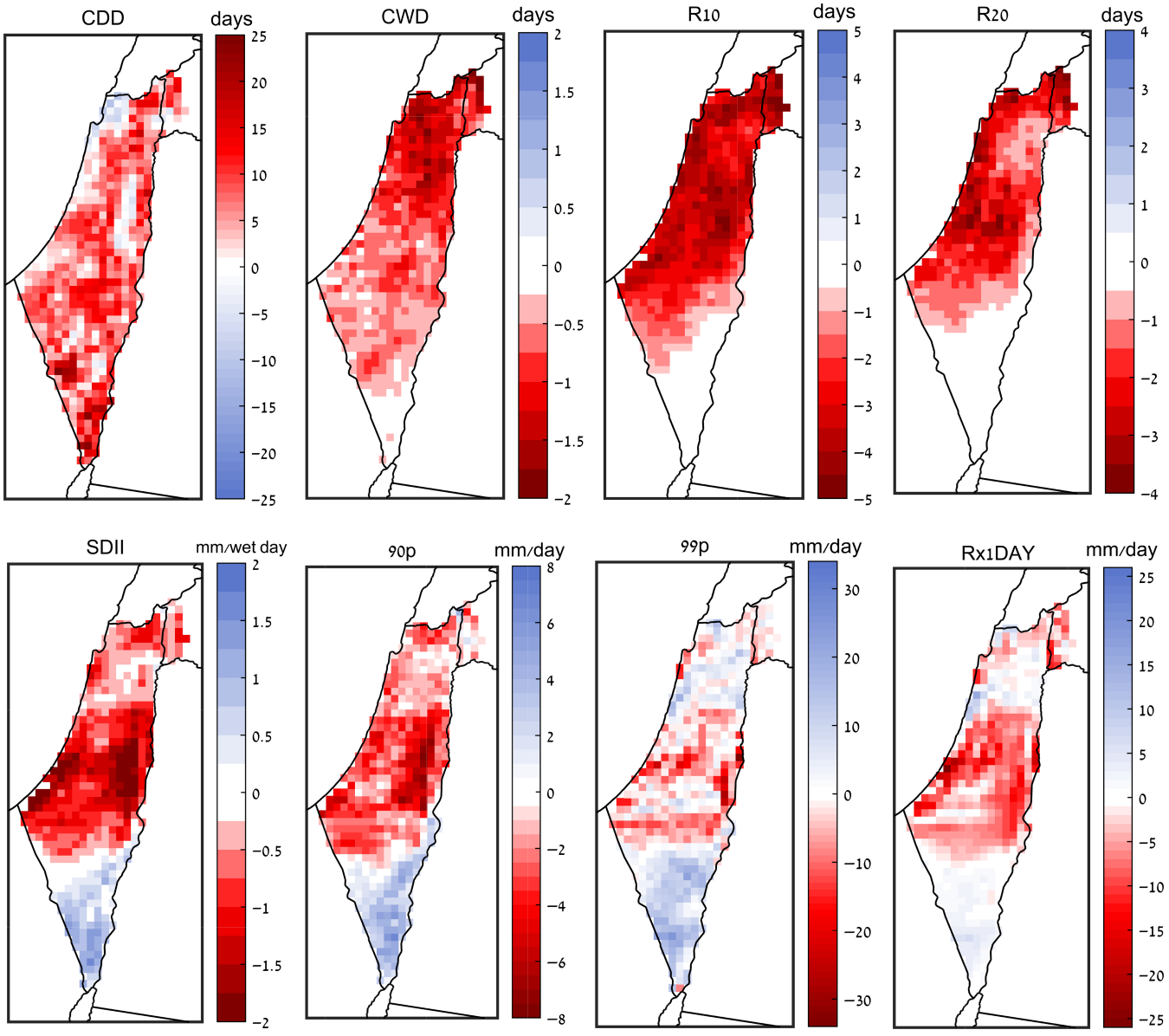

FIGURE 6 ISR8 projections for extreme precipitation indicators, for 2041–2070 minus 1981–2010, under RCP4.5 scenario Consecutive Dry Days (CDD), Consecutive Wet Days (CWD), Number of days with more than 10mm (R10), Number of days with more than 20mm (R20), Mean precipitation on wet days (SDII), 90th percentile of daily precipitation (90p), 99th percentile of daily precipitation (99p), Maximum of daily precipitation (Rx1day) [Colour figure can be viewed at wileyonlinelibrary.com]

et al. (2017b; 2017c). It should be noted that since the dry summer season in Israel lasts from May to September, the CDD index for this region represents the period between the last day of precipitation in spring and the first day in the autumn, which do not have any correlation with the daily/seasonal/annual rainfall characteristics. On the other hand, observed and projected characteristics of rainy days refer to the entire rainy period, so that, for example the CWD index represents wet spells quite well. Thus, we focused on the winter season (DJF), having more than two thirds of the annual rainfall (Saaroni *et al*., 2010). The projection of the CDD and CWD indices for DJF (Figure 7) shows a similar pattern as the annual one (Figure 6), but with different values. A general increase in CDD for DJF is shown, which is strongest in the southern part of the domain, with peaks reaching ~8 days. Also, a small decrease is demonstrated in the north. For the CWD index, a mirror image is shown with respect to CDD, that is, the largest decrease is on the northern part, with peaks reaching ~2 days and a slight increase at the southern tip. This means that shorter wet spells and longer dry periods are projected for the winter season under increased greenhouse gas concentrations.

4 | SUMMARY AND CONCLUSIONS

The main aim of this study was to project, for the first time, temperature and precipitation changes for the 21st century

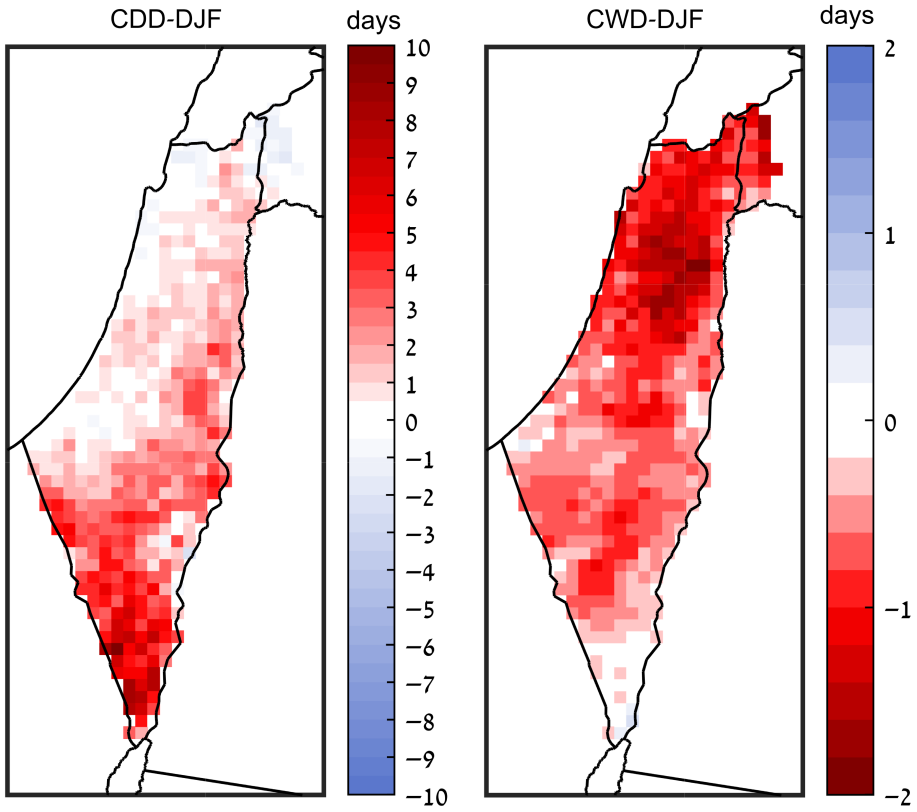

FIGURE 7 ISR8 projections for CDD for winter (DJF, left) and CWD for winter (CWD DJF, right), for 2041–2070 minus 1981–2010, under RCP4.5 scenario [Colour figure can be viewed at wileyonlinelibrary.com]

including extremes at very high resolution (about 8 km), over the region of Israel. In particular, a subset of ETCCDI indices was projected for the middle term (2041–2070) of the 21st century, under the RCP4.5 scenario. These aims were achieved by dynamically downscaling the CMCC-CM Global model with the COSMO-CLM regional model, in a configuration optimized by CMCC over the CORDEX-MENA domain (Bucchignani *et al*., 2016a; 2016b). A precondition to project extremes was to evaluate the ability of the model to assess average properties of the seasonal precipitation and temperatures. The work is based on an earlier study, which evaluated the ability of the COSMO-CLM model in representing the climatology of the subset of ETCCDI indices (Hochman *et al*., 2017a). They have shown that increasing the spatial resolution from 50 km to 8 km improves the simulation of climate and climate extremes over Israel due to the better representation of topography and the location of land and sea in the model, especially with respect to station data and for the daily extremes and less for seasonal and spatial averages.

Based on the relatively good representation of current conditions, future projections were derived here. It was shown that a general increase in seasonal mean temperatures is projected throughout the domain with peaks of ~2.5 °C, being the highest in the winter and autumn, when comparing the period 2041–2070 and 1981–2010. All extreme temperature indices project a significant increase with larger increase in the minimum temperatures as compared with maximum temperatures.

Regarding precipitation, decreases are projected for the northern and central parts of the domain, with reductions reaching ~40% in autumn, and an increase of the same order of magnitude for the most southern arid part, for the winter and spring seasons. Note that the absolute precipitation amounts are very different between the northern Mediterranean climate and the southern arid climate; the region showing projected reductions in precipitation is larger than the region showing increases. An interesting and more complex spatial pattern arises from the high-resolution simulation of extreme precipitation indicators. A projected tendency towards drier conditions is confirmed by the simulation for the Mediterranean climate and semi-arid climate of Israel, in agreement with low-resolution projections (Samuels *et al*., 2017). However, an increase in precipitation intensity is shown mostly for the southern arid part of the region that may be attributed to increase in the occurrence of active RST. For the 99th percentile of daily precipitation (99p) indications of increases (i.e., extremity) are also seen for the northern part of the country. This features can be captured only by high-resolution simulations, and could not be captured by the global models in earlier projections of extreme precipitation (e.g., Samuels *et al*., 2013, 2017) but also with regional models at lower resolution (e.g., Önol and Semazzi, 2009; Smiatek *et al*., 2011; Bozkurt *et al*., 2012). The

general decrease in precipitation probably results from the decrease already seen and projected in cyclones occurrence (e.g., Tamarin-Brodsky and Kaspi, 2017; Hochman *et al*., 2017b), which mainly influence the northern and central parts of Israel.

The work described in this study is an ongoing joint Italian–Israeli research effort, focusing on assessing the impacts of climate change, especially precipitation and temperature on fresh water resources in the EM. This is necessary for identifying and projecting socioeconomic and environmental vulnerability caused by climate change. The outcomes of this study and the ones to follow, will serve as a basis for priority setting and policy formulation towards climate adaptation at the regional level.

ACKNOWLEDGEMENTS

This work was performed within the framework of the GEMINA project, funded by the Italian Ministry of Education and the Italian Ministry of the Environment, Land and Sea. It was also supported by the Ministry of Science and Technology (MOST) of the state of Israel, by the Tel-Aviv University (TAU) President and Mintz foundation and by the Porter School of Environmental Studies at TAU. The German Helmholtz Association is gratefully acknowledged for partly funding this project within the Virtual Institute DESERVE (Dead Sea Research Venue) under contract number VH-VI-527. This article is a contribution to the HyMex society.

ORCID

Assaf Hochman http://orcid.org/0000-0002-9881-1893
Hadas Saaroni http://orcid.org/0000-0001-6369-1847

REFERENCES

Alpert, P. and Reisin, T. (1986) An early winter polar air mass penetration to the eastern Mediterranean. *Monthly Weather Review*, 114, 1411–1418.

Alpert, P., Ben-Gai, T., Baharad, A., Benjamini, Y., Yekutieli, D., Colacino, M., Diodato, L., Ramis, C., Homar, V., Romero, R., Michaelides, S. and Manes, A. (2002) The paradoxical increase of Mediterranean extreme daily rainfall in spite of decrease in total values. *Geophysical Research Letters*, 29, 1536. https://doi.org/10.1029/2001GL013554.

Alpert, P., Price, C., Krichak, S.O., Ziv, B., Saaroni, H., Osetinsky, I., Barkan, J. and Kishcha, P. (2005) Tropical tele-connections to the Mediterranean climate and weather. *Advances in Geosciences*, 2, 157–160.

Alpert, P., Krichak, S.O., Dayan, M. and Shafir, H. (2006) Climatic trends over the eastern Mediterranean: past and future projections. *CLIVAR Exchanges*, 11(2), 12–13.

Alpert, P., Krichak, S.O., Shafir, H., Haim, D. and Osetinsky, I. (2008) Climatic trends to extremes employing regional modeling and statistical interpretation over the E. Mediterranean. *Global and Planetary Change*, 63, 163–170.

Baldauf, M., Seifert, A., Förstner, J., Majewski, D., Raschendorfer, M. and Reinhardt, T. (2011) Operational convective-scale numerical weather prediction with the COSMO model: description and sensitivities. *Monthly Weather Review*, 139, 3887–3905. https://doi.org/10.1175/MWR-D-10-05013.1.

Ben-Gai, T., Bitan, A., Manes, A., Alpert, P. and Rubin, S. (1999) Temporal and spatial trends of temperature patterns in Israel. *Theoretical and Applied Climatology*, 64, 163–177.

Bozkurt, D., Turukonglu, U., Lutfi Sen, O., Önol, B. and Dalfes, H.N. (2012) Downscaled simulations of the ECHAM5, CCSM3 and HadCM3 global models for the eastern Mediterranean–Black Sea region: evaluation of the reference period. *Climate Dynamics*, 39, 207–225. https://doi.org/10.1007/s00382-011-1187-x.

Bucchignani, E., Cattaneo, L., Panitz, H.J. and Mercogliano, P. (2016a) Sensitivity analysis with the regional climate model COSMO-CLM over the CORDEX-MENA domain. *Meteorology and Atmospheric Physics*, 128(1), 73–95. https://doi.org/10.1007/s00703-015-0403-3.

Bucchignani, E., Mercogliano, P., Rianna, G. and Panitz, H.J. (2016b) Analysis of ERA-Interim driven COSMO-CLM simulations over Middle East–North Africa domain at different spatial resolutions. *International Journal of Climatology*, 36(9), 3346–3369. https://doi.org/10.1002/joc.4559.

Bucchignani, E., Mercogliano, P., Panitz, H.J. and Montesarchio, M. (2018) Climate change projections for the Middle East–North Africa domain with COSMO-CLM at different spatial resolutions. *Advances in Climate Change Research*, 9, 66–80. https://doi.org/10.1016/j.accre.2018.01.004.

Dafka, S., Toreti, A., Luterbacher, J., Zanis, P., Tyrlis, E. and Xoplaki, E. (2017) On the ability of RCMs to capture the circulation pattern of Etesians. *Climate Dynamics*, 1–20. https://doi.org/10.1007/s00382-017-3977-2.

De Vries, A.J., Tyrlis, E., Edry, D., Krichak, S.O., Steil, B. and Lelieveld, J. (2013) Extreme precipitation events in the Middle East: dynamics of the Red Sea trough. *Journal of Geophysical Research: Atmospheres*, 118, 7087–7108.

Dominguez, M., Romera, R., Sánchez, E., Fita, L., Fernández, J., Jiménez-Guerrero, P., Montávez, J.P., Cabos, W.D., Liguori, G. and Gaertner, M.A. (2013) Present-climate precipitation and temperature extremes over Spain from a set of high resolution RCMs. *Climate Research*, 58, 149–164. https://doi.org/10.3354/cr01186.

Eichler, T.P., Gaggini, N. and Pan, Z. (2013) Impacts of global warming on Northern Hemisphere winter storm tracks in the CMIP5 model suite. *Journal of Geophysical Research: Atmosphere*, 118(10), 3919–3932. https://doi.org/10.1002/jgrd.50286.

Giorgi, F., Jones, C. and Asrar, G.R. (2009) Addressing climate information needs at the regional level: the CORDEX framework. *WMO Bulletin*, 58, 175.

Giorgi, F. and Gutowski, W.J. (2015) Regional dynamical downscaling and the CORDEX initiative. *Annual Review of Environment and Resources*, 40, 467–490.

Haylock, M.R., Hofstra, N., Klein Tank, A.M.G., Klok, E.J., Jones, P.D. and New, M. (2008) A European daily high-resolution gridded dataset of surface temperature and precipitation. *Journal of Geophysical Research: Atmospheres*, 113, D20119. https://doi.org/10.1029/2008JD10201.

Held, I.M. and Soden, B.J. (2006) Robust responses of the hydrological cycle to global warming. *Journal of Climate*, 19, 5686–5699.

Hochman, A., Bucchignani, E., Gershtein, G., Krichak, S.O., Alpert, P., Levi, Y., Yosef, Y., Carmona, Y., Breitgand, J. and Mercogliano, P. (2017a) Evaluation of regional COSMO-CLM climate simulations over the eastern Mediterranean for the period 1979–2011. *International Journal of Climatology.*, 38, 1161–1176. https://doi.org/10.1002/joc.5232.

Hochman, A., Harpaz, T., Saaroni, H. and Alpert, P. (2017b) Synoptic classification in 21st century CMIP5 predictions over the eastern Mediterranean with focus on cyclones. *International Journal of Climatology.*, 38, 1476–1483. https://doi.org/10.1002/joc.5260.

Hochman, A., Harpaz, T., Saaroni, H. and Alpert, P. (2017c) The seasons' length in 21st century CMIP5 projections over the eastern Mediterranean. *International Journal of Climatology*,38(6), 2627–2637. https://doi.org/10.1002/joc.5448.

Kelley, C.P., Mohtadi, S., Cane, M.A., Seager, R. and Kushnir, Y. (2015) Climate change in the Fertile Crescent and implications of the recent Syrian drought. *Proceedings of the National Academy of Sciences of the United States of America*, 112, 3241–3246. https://doi.org/10.1073/pnas.1421533112.

Klein-Tank, A.M.G., Zwiers, F.W. and Zhang, X. (2009) *Guidelines on analysis of extremes in a changing climate in support of informed decisions for adaptation*. Geneva: Word Meteorological Organization. Climate Data and Monitoring, WCDMP-No. 72, WMO-TD No. 1500.

Krichak, S.O., Alpert, P. and Dayan, M. (2004) The role of atmospheric processes associated with Hurricane Olga in the December 2001 floods in Israel. *Journal of Hydrometeorology*, 5, 1259–1270. https://doi.org/10.1175/JHM-399.1.

Krichak, S.O., Alpert, P. and Kunin, P. (2010) Numerical simulation of seasonal distribution of precipitation over the eastern Mediterranean with a RCM. *Climate Dynamics*, 34(1), 47–59.

Krichak, S.O., Barkan, J., Breitgard, J.S., Gualdi, S. and Feldstein, S.B. (2015) The role of the export of tropical moisture into midlatitudes for extreme precipitation events in the eastern Mediterranean region. *Theoretical and Applied Climatology*, 121, 499–515.

Laprise, R., Hernández-Díaz, L., Tete, K., Sushama, L., Šeparović, L., Martynov, A., Winger, K. and Valin, M. (2013) Climate projections over CORDEX Africa domain using the fifth-generation Canadian regional climate model (CRCM5). *Climate Dynamics*, 41(11–12), 3219–3246. https://doi.org/10.1007/s00382-012-1651-2.

Lawrence, P.J. and Chase, T.N. (2007) Representing a new MODIS consistent land surface in the community land model (CLM 3.0). *Journal of Geophysical Research*, 112(G1), G01023. https://doi.org/10.1029/2006JG000168.

Lelieveld, J., Proestos, Y., Hadjinicolaou, P., Tanarhte, M., Tyrlis, E. and Zittis, G. (2016) Strongly increasing heat extremes in the Middle East and North Africa (MENA) in the 21st century. *Climatic Change*, 137(1), 245–260. https://doi.org/10.1007/s10584-016-1665-6.

Levi, Y., Shilo, E. and Setter, I. (2011) Climatology of a summer coastal boundary layer with 1290-MHz wind profiler radar and a WRF simulation. *Journal of Applied Meteorology and Climatology*, 50(9), 1815–1826.

Lionello, A.F., Gacic, M., Planton, S., Trigo, R. and Ulbrich, U. (2014) The climate of the Mediterranean region: research progress and climate change impacts. *Regional Environmental Change*, 14, 1679–1684.

Lu, J., Vecchi, G.A. and Reichler, T. (2007) Expansion of the Hadley cell under global warming. *Geophysical Research Letters*, 34, L06805. https://doi.org/10.1029/2006GL028443.

Moss, R., Edmonds, J., Hibbard, K., Manning, M., Rose, S., Van Vuuren, D.P., Carter, T., Emori, S., Kainuma, M., Kram, T., Meehl, G., Mitchell, J., Nakicenovic, N., Riahi, K., Smith, S., Stouffer, R., Thomson, A., Weyant, J. and Wilbanks, T. (2010) The next generation of scenarios for climate change research and assessment. *Nature*, 463, 747–756. https://doi.org/10.1038/nature08823.

Önol, B. and Semazzi, F.H.M. (2009) Regionalization of climate change simulations over the eastern Mediterranean. *Journal of Climate*, 22, 1944–1961. https://doi.org/10.1175/2008JCLI1807.1.

Ozturk, T., Tufan Turp, M., Türkeş, M. and Levent Kurnaz, M. (2018) Future projections of temperature and precipitation climatology for CORDEX-MENA domain using RegCM4.4. *Atmospheric Research*, 206, 87–107. https://doi.org/10.1016/j.atmosres.2018.02.009.

Rockel, B., Will, A. and Hense, A. (2008) The regional climate model COSMO-CLM (CCLM). *Meteorologische Zeitschrift*, 17, 347–348. https://doi.org/10.1127/0941-2948/2008/0309.

Rostkier-Edelstein, D., Kunin, P., Hopson, T.M., Yubao, L. and Givati, A. (2015) Statistical downscaling of seasonal precipitation in Israel. *International Journal of Climatology*, 36, 590–606.

Saaroni, H., Bitan, A., Alpert, P. and Ziv, B. (1996) Continental polar outbreaks into the Levant and eastern Mediterranean. *International Journal of Climatology*, 16, 1175–1191.

Saaroni, H., Halfon, N., Ziv, B., Alpert, P. and Kutiel, H. (2010) Links between the rainfall regime in Israel and location and intensity of Cyprus lows. *International Journal of Climatology*, 30, 1014–1025.

Saaroni, H., Ziv, B., Lempert, J., Gazit, Y. and Morin, E. (2015) Prolonged dry spells in the Levant region: climatological–synoptic analysis. *International Journal of Climatology*, 35, 2223–2236.

Samuels, R., Smiatek, G., Krichak, S., Kunstmann, H. and Alpert, P. (2011) Extreme value indicators in highly resolved climate change simulations for the Jordan River area. *Journal of Geophysical Research*, 116, D24123. https://doi.org/10.1029/2011JD016322.

Samuels, R., Harel, M. and Alpert, P. (2013) A new methodology for weighting high resolution model simulations to project future rainfall in the Middle East. *Climate Research*, 57, 51–60. https://doi.org/10.3354/cr01147.

Samuels, R., Hochman, A., Baharad, A., Givati, A., Levi, Y., Yosef, Y., Saaroni, H., Ziv, B., Harpaz, T. and Alpert, P. (2017) Evaluation and projection of extreme precipitation indices in the eastern Mediterranean based on CMIP5 multi-model ensemble. *International Journal of Climatology.*, 38, 2280–2297. https://doi.org/10.1002/joc.5334.

Scoccimarro, E., Gualdi, S., Bellucci, A., Sanna, A., Fogli, P.G., Manzini, E., Vichi, M., Oddo, P. and Navarra, A. (2011) Effects of tropical cyclones on ocean heat transport in a high resolution coupled general circulation model. *Journal of Climate*, 24, 4368–4384.

Seidel, D.J., Fu, Q., Randel, W.J. and Reichler, T.J. (2008) Widening of the tropical belt in a changing climate. *Nature Geoscience*, 1(1), 21–24. https://doi.org/10.1038/ngeo.2007.38.

Seneviratne, S.I., Corti, T., Davin, E.L., Hirschi, M., Jaeger, E.B., Lehner, I., Orlowsky, B. and Teuling, A.J. (2010) Investigating soil moisture–climate interactions in a changing climate: a review. *Earth Science Reviews*, 99(3–4), 125–161. https://doi.org/10.1016/j.earscirev.2010.02.004.

Smiatek, G., Kunstmann, H. and Heckl, A. (2011) High resolution climate change simulations for the Jordan River area. *Journal of Geophysical Research*, 116, D16111. https://doi.org/10.1029/2010JD015313.

Soares, P.M.M., Cardoso, R.M., Miranda, P.M.A., Viterbo, P. and Belo-Pereira, M. (2012) Assessment of the ENSEMBLES regional climate models in the representation of precipitation variability and extremes over Portugal. *Journal of Geophysical Research*, 117, D07114. https://doi.org/10.1029/2011JD016768.

Steppeler, J., Doms, G., Schättler, U., Bitzer, H.W., Gassmann, A., Damrath, A. and Gregoric, G. (2003) Meso-gamma scale forecasts using the non-hydrostatic model LM. *Meteorology and Atmospheric Physics*, 82, 75–96. https://doi.org/10.1007/s00703-001-0592-9.

Sutton, R.T., Dong, B. and Gregory, J.M. (2007) Land/sea warming ratio in response to climate change: IPCC AR4 model results and comparison with observations. *Geophysical Research Letters*, 34, L02701. https://doi.org/10.1029/2006GL028164.

Tamarin-Brodsky, T. and Kaspi, Y. (2017) Enhanced poleward propagation of storms under climate change. *Nature Geoscience*, 10, 908–913.

Tanarhte, M., Hadjinicolaou, P. and Lelieveld, J. (2012) Intercomparison of temperature and precipitation data sets based on observations in the Mediterranean and the Middle East. *Journal of Geophysical Research*, 117, D12102. https://doi.org/10.1029/2011JD017293.

Tegen, I., Hollrig, P., Chin, M., Fung, I., Jacob, D. and Penner, J. (1997) Contribution of different aerosol species to the global aerosol extinction optical thickness: estimates from model results. *Journal of Geophysical Research*, 102, 895–915. https://doi.org/10.1029/97JD01864.

Tiedtke, M. (1989) A comprehensive mass flux scheme for cumulus parameterization in large-scale models. *Monthly Weather Review*, 117, 1779–1800.

Turco, M., Zollo, A.L., Ronchi, C., De Luigi, C. and Mercogliano, P. (2013) Assessing gridded observations for daily precipitation extremes in the Alps with a focus on northwest Italy. *Natural Hazards and Earth System Sciences*, 13, 1457–1468. https://doi.org/10.5194/nhess-13-1457-2013.

Wilby, R.L. and Wigley, T.M.L. (1997) Downscaling general circulation model output: a review of methods and limitations. *Progressions in Physical Geography*, 21, 530–548.

Yatagai, A., Alpert, P. and Xie, P. (2008) Development of a daily gridded precipitation data set for the Middle East. *Advances in Geosciences*, 12, 1–6.

Yatagai, A., Kamiguchi, K., Arakawa, O., Hamada, A., Yasutomi, N. and Kitoh, A. (2012) APHRODITE: constructing a long-term daily gridded precipitation dataset for Asia based on a dense network of rain gauges. *Bulletin of the American Meteorological Society*, 93, 1401–1415.

Yosef, Y., Saaroni, H. and Alpert, P. (2009) Trends in daily rainfall intensity over Israel 1950/1-2003/4. *The Open Atmospheric Science Journal*, 3, 196–203.

Zhang, X., Aguilar, E., Sensoy, S., Melkonyan, H., Tagiyeva, U., Ahmed, N., Kutaladze, N., Rahimzadeh, F., Taghipour, A., Hantosh, T.H., Albert, P., Semawi, M., Karam Ali, M., Said al-Shabibi, M.H., al-Oulan, Z., Zatari, T., al Dean Khelet, I., Hamoud, S., Sagir, R., Demircan, M., Eken, M., Adiguzel, M., Alexander, L., Peterson, T.C. and Wallis, T. (2005) Trends in Middle East climate extreme indices from 1950–2003. *Journal of Geophysical Research*, 110, D22104. https://doi.org/10.1029/2005JD006181.

Zhang, X., Alexander, L., Hegerl, C., Jones, P., Tank, A.K., Peterson, T.C., Trewin, B. and Zwiers, F.W. (2011) Indices for monitoring changes in extremes based on daily temperature and precipitation data. *Climatic Change*, 2, 851–870.

Zittis, G., Hadjinicolaou, P. and Lelieveld, J. (2014) Role of soil moisture in the amplification of climate warming in the eastern Mediterranean and the Middle East. *Climate Research*, 59(1), 27–37.

Zittis, G. (2017) Observed rainfall trends and precipitation uncertainty in the vicinity of the Mediterranean, Middle East and North Africa. *Theoretical and Applied Climatology*, 1–24. https://doi.org/10.1007/s00704-017-2333-0.

Zittis, G., Bruggeman, A., Camera, C., Hadjinicolaou, P. and Lelieveld, J. (2017) The added value of convection permitting simulations of extreme precipitation events over the eastern Mediterranean. *Atmospheric Research*, 191, 20–33. https://doi.org/10.1016/j.atmosres.2017.03.002.

Ziv, B., Saaroni, H., Baharad, A., Yekutieli, D. and Alpert, P. (2005) Indications for aggravation in summer heat conditions over the Mediterranean Basin. *Geophysical Research Letters*, 32, L12706. https://doi.org/10.1029/2005GL022796.

Ziv, B., Saaroni, H., Pargament, R., Harpaz, T. and Alpert, P. (2014) Trends in the rainfall regime over Israel, 1975–2010, and their relationship to large-scale variability. *Regional Environmental Change*, 14(5), 1751–1764. https://doi.org/10.1007/s10113-013-0414-x.

Zollo, A.L., Rillo, V., Buchignani, E., Montesarchio, M. and Mercogliano, P. (2016) Extreme temperature and precipitation events over Italy: assessment with high-resolution simulations with COSMO-CLM and future scenarios. *International Journal of Climatology*, 36(2), 987–1005. https://doi.org/10.1002/joc.4401.

How to cite this article: Hochman A, Mercogliano P, Alpert P, Saaroni H, Bucchignani E. High-resolution projection of climate change and extremity over Israel using COSMO-CLM. *Int J Climatol*. 2018;1–12. https://doi.org/10.1002/joc.5714